J|A|C|S COMMUNICATIONS

Published on Web 05/27/2009

Distance Dependence of Plasmon-Enhanced Photocurrent in Dye-Sensitized Solar Cells

Stacey D. Standridge, George C. Schatz, and Joseph T. Hupp*

Department of Chemistry, Northwestern University, 2145 Sheridan Road, Evanston, Illinois, 60208-3113

Received March 25, 2009; E-mail: j-hupp@northwestern.edu

Dye-sensitized solar cells (DSSCs) represent one of the most promising emerging technologies for light-to-electrical energy conversion.[1−4] Among the most attractive potential features of DSSCs are (a) minimal capital costs for synthesis of component materials and (b) ease and economy of fabrication. The operation of DSSCs is based on the division of the light collection and charge separation functions in the cell. The anode consists of a transparent nanoparticulate TiO_2 (or other metal-oxide) network that is sensitized with a molecular dye. Upon the absorption of light, the dye injects an electron into the TiO_2 network. The electron travels through this network until it is collected. The resulting dye radical is reduced to its ground state by a redox-based mediator, which is typically I^-/I_3^-.

Despite intense research efforts, however, the highest reported efficiencies for DSSCs (ca. 11%) are only slightly higher than those achieved in the mid-1990s.[5] While improvements in photocurrent and fill factor can be envisioned, the greatest possibilities for efficiency gains are likely to be those that center on increasing the photovoltage.[3] One approach to decreasing the dark current, and thus increasing the photovoltage, lies in reducing the surface area of the TiO_2 network, as the dark current is directly proportional to the photoelectrode surface area.[6] However, any decrease in surface area must be accompanied by a concomitant increase in dye extinction to offset losses in photocurrent from a lower dye loading. Indeed, much effort has been devoted to developing more efficient dyes.[7,8] In the present study, we demonstrate the use of plasmonic particles in DSSCs to increase the extinction of the "N3" dye (*cis*-bis-(4,4′-dicarboxy-2,2′-bipyridine) dithiocyanato ruthenium(II)).

Plasmons are created when incident light excites coherent oscillation of the free electrons in metal nanoparticles (NPs), typically composed of silver or gold.[9] This phenomenon gives rise to unique properties, such as an intense absorption feature and an enhanced electromagnetic field, that have been implemented in a variety of applications ranging from sensing to enhanced fluorescence.[10−13] Although not thoroughly investigated, the concept of using plasmon-enhanced dye absorption in DSSCs has been introduced in the literature.[14−16] In the typical experiment, the silver NPs were in contact with both the dye and the Co(1,10-phenanthoroline)$_3^{2+/3+}$-based electrolyte. A small increase in the photocurrent was observed at longer wavelengths.[16] However, unpublished experiments in our lab have demonstrated that a similar Co(4,4′-di-*tert*-butyl-2,2′-dipyridyl)$_3^{2+/3+}$-based electrolyte etches silver NPs.

We recently reported the use of atomic layer deposition (ALD) to conformally coat silver NPs with a protective layer of TiO_2.[17] We found that 300 cycles (7.7 nm) of anatase TiO_2 were required to protect the particles from the corrosive I^-/I_3^- solution. Separately, we have recently shown that *amorphous* TiO_2 affords efficient electron transport in DSSCs, provided that the layer of TiO_2 between the dye and the charge collector is sufficiently thin.[18] Based on this result, the thickness of amorphous TiO_2 required to protect silver NPs was investigated. Experiments analogous to those in the previous study[17] indicate that as little as 2.0 nm of amorphous TiO_2 are adequate to form a pinhole free layer on silver NPs.

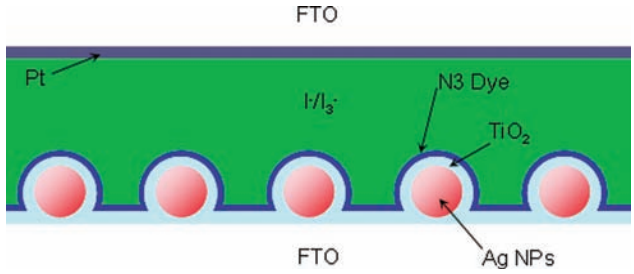

Figure 1. Configuration of solar cells containing silver NPs and dye.

As the distance between a dye molecule and a plasmonic particle increases, the plasmon-enhanced extinction of the dye decreases due to the decaying electromagnetic field. In the context of DSSCs, the plasmon-enhanced photocurrent should accordingly diminish as the spacer layer between the dye and the silver NPs increases. This theoretical distance dependence of plasmon-enhanced photocurrent in DSSCs is the basis of the study reported herein. ALD was employed to coat flat photoanodes conformally with 2.0−4.9 nm of amorphous TiO_2 or 6.5−8.0 nm of anatase TiO_2. The anatase form was obtained by annealing the amorphous as-deposited oxide at 450 °C for 30 min.[17] For every TiO_2 thickness investigated, three electrodes (one with only dye, one with only silver, and one with both dye and silver) were fabricated, and spectral properties of the anodes were recorded before cell assembly. Silver particles were spherical with a diameter = 36 ± 3 nm. The configuration of cells containing both dye and silver is shown in Figure 1. A thorough description of the experimental methods used is given in the Supporting Information (SI).

The optical properties of the photoanodes are summarized in Figure 2. Figure 2a illustrates the extinction of the plasmonic substrates before the dye is attached. As expected, the plasmon extinction intensifies and red-shifts as the thickness of amorphous TiO_2 increases. The extinction of the sample coated with 6.5 nm of anatase TiO_2 is slightly red-shifted and higher in intensity than the analogous amorphous sample. The spectra of the remaining anatase samples are omitted for clarity. However, the plasmon shift is saturated after deposition of ca. 6.5 nm of anatase. The extinction spectrum of N3 absorbed onto a silver-free substrate is included for comparison. The spectral overlap between the dye and the plasmon is evident, particularly for the sample featuring a 2.0 nm layer of amorphous TiO_2.

The extinction spectra of the anodes before and after dye attachment were subtracted to approximate the extinction of the dye. The difference spectrum for the dye on a bare substrate is included at the bottom of Figure 2a. Dye loading (and therefore,

extinction) was consistently less on the anatase substrates than on amorphous TiO_2. Difference spectra for dye attached to the silver-containing substrates are shown in Figure 2b. As the thickness of the TiO_2 increases, the extinction of the dye decreases and red-shifts. This drastic reduction in the plasmon-enhanced extinction of the dye is the product of two distinct effects. First, as the plasmon red-shifts, the spectral overlap between the plasmon and the dye diminishes (Figure 2a). Second, as the TiO_2 layer increases in thickness, the electromagnetic field at the dye is decreased. These effects conspire to give less plasmon-enhanced dye extinction with thicker TiO_2 layers.

A photograph of the anodes with 2.0 nm of amorphous TiO_2 is shown in Figure 2c. The sample with only a monolayer of N3 dye is nearly colorless, and the sample with only silver NPs on the substrate is pale yellow. However, the sample with the both silver NPs and dye exhibits a deep red color that is consistent with the color of N3 dye in solution. The difference spectrum for this sample is given by the solid red line in the top of Figure 2b. The peaks of this trace overlap well with the peaks of the spectrum of N3 on a silver-free electrode.

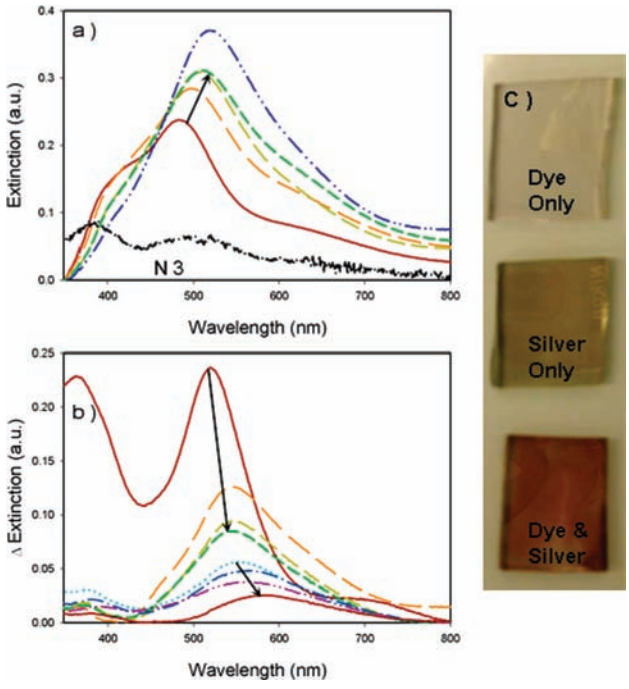

Figure 2. Optical properties of the photoanodes. (a) Evolution of the plasmon extinction as the thickness of the amorphous TiO_2 increases from 125 to 300 cycles (2.0 to 4.8 nm). The dot-dash blue line corresponds to 300 cycles of anatase TiO_2, and the black line corresponds to N3 on FTO. (b) Difference spectra of dye on silver NP substrates. The arrows indicate increasing TiO_2 thickness. The top four spectra and the bottom four spectra correspond to amorphous and anatase TiO_2, respectively. (c) Photo of anodes with 125 cycles of amorphous TiO_2.

After optical measurements were recorded, cells were assembled. Solar cell data are presented in Figure 3. A full list of the data obtained can be found in Table S2 (SI). The incident photon conversion efficiencies (IPCEs) of the samples with 125 cycles (2.0 nm) of amorphous TiO_2 are shown in Figure 3a. The sample with only silver produced no appreciable current. The sample with only dye showed a peak IPCE of ~0.2%. The shape of this curve corresponds to the extinction of the N3 dye. The cell with both silver NPs and dye had a peak IPCE value of ~1.4%. This is clearly larger than the sum of the IPCEs from the two reference cells. Open-circuit photovoltages (V_{OC}) of up to 800 mV were recorded for Ag/TiO_2/N3 cells (see SI). For comparison, champion DSSCs (N3 or N719 dye) feature V_{OC} values of 846 ± 20 mV.[4]

Figure 3b shows the evolution of the IPCEs of the cells with dye and Ag as the TiO_2 thickness increases. There is a subtle red shift, and the IPCE decreases as the TiO_2 layer is made thicker. For anatase versus amorphous oxide samples of the same thickness, the former show lower IPCEs, a consequence of the aforementioned differences in dye loading. The trends observed in Figure 3b for IPCE values correlate well with those seen in the extinction difference spectra of the same samples (Figure 2b).

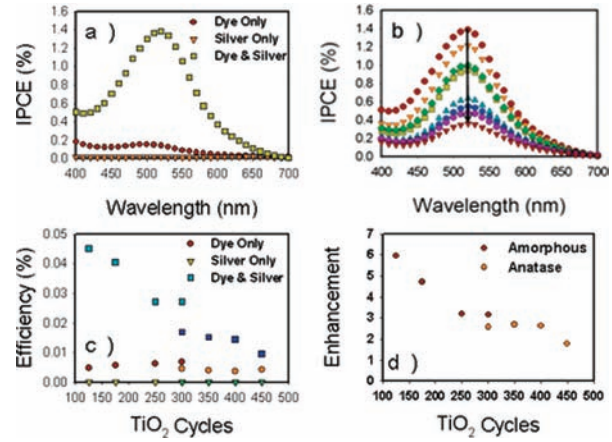

Figure 3. IPCEs and overall cell trends. (a) IPCEs for cells with 125 cycles of amorphous TiO_2. (b) IPCEs for cells with silver NPs and dye. The arrow indicates increasing TiO_2 thickness. The top four spectra and the bottom four spectra correspond to amorphous and anatase TiO_2, respectively. (c) Efficiencies of the cells. Dark blue, orange, and green symbols correspond to anatase samples. Light blue, red, and yellow symbols correspond to amorphous samples. (d) Calculated plasmon-enhancement factor as a function of TiO_2 thickness.

Cell efficiencies are presented in Figure 3c. Cells with only silver had efficiencies of essentially zero. Samples with only a monolayer of dye showed overall energy conversion efficiencies of less than 0.01%. Cells with silver NPs and dye were considerably more efficient than either of the reference cells. The best cell (2.0 nm of amorphous TiO_2) had an efficiency of ca. 0.05%. However, as the TiO_2 thickness increased, the efficiencies of the cells with both silver and dye were reduced. Notably, amorphous cells have efficiencies that are better than or equal to the efficiencies of anatase cells for similar TiO_2 thicknesses. This further confirms that, for very thin TiO_2 layers, the transport properties of amorphous TiO_2 are sufficient for DSSCs.

A plasmon-enhanced photocurrent factor was calculated using eq 1, where J_{sc} is the short-circuit current for each type of cell. The factor 1.4 in the denominator accounts for the difference in surface area, and thus dye coverage, between substrates with and without silver NPs attached. The denominator factor was calculated by using comparative dye-loading data obtained from quartz crystal microbalance (QCM) measurements (Figure S2, SI) and corroborated by AFM-based measurements of surface areas. As shown in Figure 3d, the plasmon-derived photocurrent enhancement clearly increases as the thickness of the TiO_2 decreases. The trend is attributed to stronger electromagnetic fields and better spectral overlap between the dye and the silver with thinner TiO_2 spacer layers. For the thinnest TiO_2 layer (125 cycles, 2.0 nm amorphous), the observed photocurrent is almost 6 times that of the plasmon-particle-free cell. At 560 nm, the monochromatic photocurrent enhancement is a factor of 9. The magnitude of the plasmon-enhancement of the photocurrent is striking, particularly considering

that the system is not yet optimized, with respect to either dye or plasmonic particle structure.

$$Enhancement = \frac{J_{sc(Dye+Silver)}}{(J_{sc(Dye)} \times 1.4) + J_{sc(Silver)}} \quad (1)$$

In 1996, Gratzel et al. calculated a maximum achievable IPCE of 0.27% at 530 nm for a flat anatase TiO_2 surface covered with N3 dye.[19] The cells in this study with only dye have IPCEs at 530 nm of 0.09−0.11% on anatase substrates and 0.13−0.16% on the amorphous substrates. In contrast, the cell with silver NPs and dye and the thinnest layer amorphous TiO_2 (125 cycles, 2.0 nm) had an astounding IPCE of 1.34% at 530 nm. This value decreases with increasing TiO_2 thickness until it reaches a value of 0.34% with 450 cycles (8.0 nm) of anatase TiO_2. Even this value is almost 1.3 times as large as the calculated maximum achievable IPCE. The largest observed IPCE of 1.34% is almost 5 times the maximum predicted IPCE under standard cell operating conditions. Although the silver NPs impart some increase in surface area over the flat substrates (1.4-fold), this alone is not enough to account for the larger-than-predicted IPCE values. Any accounting for the magnitude of the observed IPCE values must include plasmon-enhanced absorption by the dye.

As was previously alluded to, there is room for improvement in the present system, and much larger values of plasmon-enhanced photocurrent are theoretically achievable. For example, a further decrease in the spacing between the silver NPs and the dye would give still larger plasmon-enhanced photocurrents than observed thus far. To explore this possibility, a sample with 10 cycles (1.1 nm) of Al_2O_3 between the particles and the dye was fabricated. Al_2O_3 was chosen as the spacer material in this sample, because, relative to TiO_2, less Al_2O_3 is required to form a pinhole free layer. Figure 4 compares the difference spectra of this sample to the most efficient cell in this study (125 cycles, 2.0 nm amorphous TiO_2). The dashed line corresponds to the sample with 125 cycles of amorphous TiO_2, which gave a plasmon-enhanced photocurrent factor of ∼5.9. The solid line corresponds to the sample with 10 cycles (1.1 nm) of Al_2O_3 between the silver NPs and the N3 dye. Clearly, much larger plasmon enhancements of photocurrent should be attainable if thinner, pinhole-free TiO_2 coatings can be developed. At present, however, thinner layers offer insufficient protection of the silver particles from electrolyte-based corrosion.

In summary, we have examined the distance dependence of the plasmon-enhanced properties in DSSCs. The plasmon-enhanced extinction of the dye is most pronounced in the sample with the thinnest layer of amorphous TiO_2 (2.0 nm). The extinction of the dye red-shifts and decreases as the TiO_2 thickness increases. This trend in extinction is echoed by the observed photocurrent trends in the solar cells. The photocurrent of the cells containing both silver NPs and dye decreases as the spacer layer increases in thickness. This is ascribed to two complementary factors. First, as the TiO_2 thickness increases, the dye experiences a less intense electromagnetic field from the plasmon. A more subtle effect, however, is that the spectral overlap between the dye and the plasmon is decreased as the TiO_2 layer increases in thickness. Preliminary observations of plasmon-enhanced dye extinction with an ultrathin spacer layer (10 cycles, 1.1 nm Al_2O_3) suggest that larger gains in plasmon-enhanced photocurrent are possible.

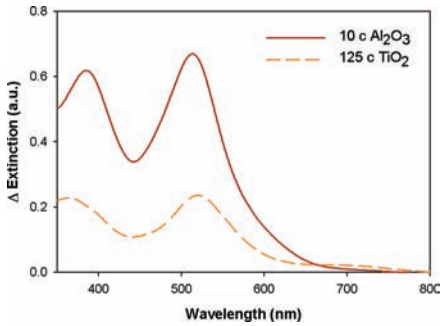

Figure 4. Approximate extinction of N3 dye on substrates with 10 cycles of Al_2O_3 (solid) and 125 cycles of amorphous TiO_2 (dashed) between silver NPs and the dye.

Acknowledgment. We thank Chaiya Prasittichai for helpful discussions and Dr. Guang Lu for QCM measurements. We thank Prof. Michael Pellin and Dr. Jeff Elam for helpful discussions and for access to ellipsometry facilities at Argonne National Laboratory. SEM measurements were performed in the EPIC facilities of the NUANCE Center at Northwestern University. The NUANCE Center is supported by NSF-NSEC, NSF-MRSEC, Keck Foundation, the State of Illinois, and Northwestern University. We gratefully acknowledge financial support from the U.S. Dept. of Energy, Office of Science (Grant Nos. DE-FG87ER13808 and DE-FG02-03-ER15487). S.D.S. wishes to thank the NWUIOA.

Supporting Information Available: Experimental procedures, SEM micrograph of anode before device fabrication, TiO_2 thicknesses, solar cell data, and QCM measurements. This material is available free of charge via the Internet at http://pubs.acs.org.

References

(1) Ardo, S.; Meyer, G. J. *Chem. Soc. Rev.* **2009**, *38*, 115–164.
(2) O'Regan, B.; Gratzel, M. *Nature* **1991**, *353*, 737–740.
(3) Nelson, J. *The Physics of Solar Cells*; Imperial College Press: London, 2003.
(4) Martinson, A. B. F.; Hamann, T. W.; Pellin, M. J.; Hupp, J. T. *Chem.—Eur. J.* **2008**, *14*, 4458–4467.
(5) Nazeeruddin, M. K.; DeAngelis, F.; Fantacci, S.; Selloni, A.; Viscardi, G.; Liska, P.; Ito, S.; Takeru, B.; Gratzel, M. *J. Am. Chem. Soc.* **2005**, *127*, 16835–16847.
(6) Zhu, K.; Kopidakis, N.; Neale, N. R.; van de Lagemaat, J.; Frank, A. J. *J. Phys. Chem. B* **2006**, *110*, 25174–25180.
(7) Hamann, T. W.; Jensen, R. A.; Martinson, A. B. F.; Van Ryswyk, H.; Hupp, J. T. *Energy Environ. Sci.* **2008**, *1*, 66–78.
(8) Youm, K.-T.; Nguyen, S. T.; Hupp, J. T. *Chem. Commun.* **2008**, *29*, 3375–3377.
(9) Kelly, K. L.; Coronado, E.; Zhao, L. L.; Schatz, G. C. *J. Phys. Chem. B* **2003**, *107*, 668–677.
(10) Pan, S.; Rothberg, L. J. *J. Am. Chem. Soc.* **2005**, *127*, 6087–6094.
(11) Zhao, J.; Jensen, L.; Sung, J.; Zou, S.; Schatz, G. C.; VanDuyne, R. P. *J. Am. Chem. Soc.* **2007**, *129*, 7647–7656.
(12) Lakowicz, J. R.; Shen, Y.; D'Auria, S.; Malicka, J.; Fang, J.; Gryczynski, Z.; Gryczynski, I. *Anal. Biochem.* **2002**, *301*, 261–277.
(13) Aslan, K.; Wu, M.; Lakowicz, J. R.; Geddes, C. D. *J. Am. Chem. Soc.* **2007**, *129*, 1524–1525.
(14) Zhao, G.; Kozuka, H.; Yoko, T. *Sol. Energy Mater. Sol. Cells* **1997**, *46*, 219–231.
(15) Wen, C.; Ishikawa, K.; Kishima, M.; Yamada, K. *Sol. Energy Mater. Sol. Cells* **2000**, *61*, 339–351.
(16) Ishikawa, K.; Wen, C.-J.; Yamada, K.; Okubo, T. *J. Chem. Eng. Jpn.* **2004**, *37*, 645–649.
(17) Standridge, S. D.; Schatz, G. C.; Hupp, J. T. *Langmuir* **2009**, *25*, 2596–2600.
(18) Martinson, A. B. F.; Elam, J. W.; Liu, J.; Hupp, J. T.; Pellin, M. J.; Marks, T. J. *Nano Lett.* **2008**, *8*, 2862–2866.
(19) Kavan, L.; Gratzel, M.; Gilbert, S. E.; Klemenz, C.; Scheel, H. J. *J. Am. Chem. Soc.* **1996**, *118*, 6716–6723.

JA9022072